ISBN: 978-3-95450-227-1 ISSN: 2673-5490 doi:10.18429/JACoW-IPAC2022-WEPOPT065

SIMULATIONS OF THE UPGRADED DRIVE-BEAM PHOTOINJECTOR AT THE ARGONNE WAKEFIELD ACCELERATOR

E. Frame[1*], S. Doran[2], S. Kim[2], X. Lu[1,2], P. Piot[1,2], J. G. Power[2], E. E. Wisniewski[2]
[1]Northern Illinois University, DeKalb, IL, USA
[2]Argonne National Laboratory, Lemont, IL, USA

Abstract

The Argonne Wakefield Accelerator (AWA) is planning to upgrade the photoinjector of its drive-beam accelerator. The main goal of the upgrade is to improve the beam brightness using a symmetrized RF-gun cavity and linac cavities. In the process, the photoinjector is reconfigured and some of the solenoid magnets will be redesigned. A challenging aspect of this optimization is that the injector should be able to produce bright low-charge (~ 1 nC) bunches while also being capable of operating with high-charge (~ 50 nC) bunches. This paper discusses the optimization of the beam dynamics for the low- and high-charge cases and explores the performances of the proposed configuration.

INTRODUCTION

At the Argonne Wakefield Accelerator (AWA), the drive-beam photoinjector is the backbone of the facility [1]. The photoinjector generates ≤ 70-MeV electron bunches in either a low-charge or high-charge regime. In the low-charge mode, single bunches with charge ≤ 1 nC are produced with an emphasis on forming low-emittance bunches to support various beam-dynamics experiments including beam-driven wakefield acceleration in THz structures. In the high-charge regime, bunches train comprising eight 50-nC bunches are produced and principally employed to excite fields in power extraction and transfer structures (PETS). These structures produce high-power (sub-GW), high-frequency (X-band and above) electromagnetic radiation to power high-frequency accelerating structures in the so-called two-beam acceleration (TBA) scheme [2, 3]. Over the last few years, AWA has increased its focus on developing methods to control bright beams [4]. Correspondingly, the AWA accelerator will be upgraded to enable the generation of low-emittance, low-charge electron beams.

LOW-ENERGY SECTION UPGRADE

The AWA drive-beam linac comprises a $1 + \frac{1}{2}$-cell 1.3-GHz RF gun surrounded by three solenoidal lenses, followed by a linac consisting of seven 1.3-GHz 7-cell standing-wave structures [1]. The low-energy section upgrade is primarily driven by the installation of a symmetrized RF gun to reduce the time-dependent kick produced by the sided input-power coupler. The kick is responsible for emittance growth and possible coupling as it occurs in a region with an axial magnetic field produced by solenoid lenses. In this report, we investigate possible configurations for one of the solenoid lenses (the "matching" solenoid located downstream of the RF gun) constrained by mechanical assembly and real-estate requirements and motivated by improving the beam brightness. Both the low- and high-charge regimes are explored and trade-off between the different designs are considered. In its current configuration, the "matching" solenoid installed immediately downstream of the RF gun has two iron plates fastened on each side to reduce the magnetic field fringe field while accommodating constraints that came from the beamline itself. However, these metallic plates generate a non-cylindrically symmetric magnetic field that negatively impacts the beam dynamics. The motivation behind the change in the solenoid design is to eliminate this field asymmetry and to possibly change the position of the solenoid. Two new solenoid designs were considered for this upgrade. One of the designs ("Design 1") is similar to the solenoid that is currently installed at AWA - the only difference being that the metal plates are removed. Due to the size of the bore, this solenoid is constrained to one position on the beamline (0.273 m downstream of the photocathode). The other design ("Design 2") has a larger bore which allows the position of the solenoid center to vary within $z_s \in [0.273, 0.330]$ m from the photocathode. The corresponding axial magnetic fields $B_z(r = 0, z)$ appear in Fig. 1(a).

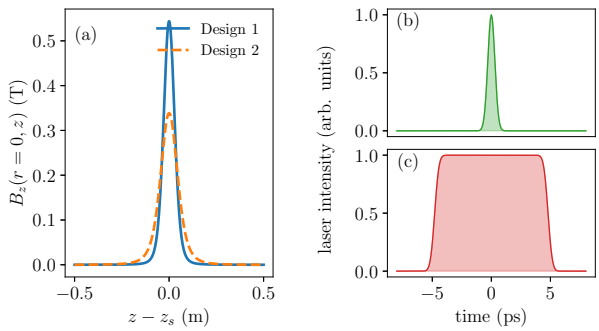

Figure 1: Comparison of the axial field produced by the two matching solenoid designs (a) and laser temporal profile for the Gaussian "1G" (b) and flat top "FT" (c) distributions.

SIMULATIONS & OPTIMIZATION

The goal of the optimization is to understand the trade-off between the transverse emittance $\varepsilon_\perp$ and rms energy spread σ_E. Given that AWA does not include any compression scheme, these two parameters are the most relevant to a number of applications often considered at AWA. Low-

* eframe@anl.gov

ISBN: 978-3-95450-227-1 ISSN: 2673-5490 doi:10.18429/JACoW-IPAC2022-WEPOPT065

emittance [$O(1)$ μm], low-charge [$O(1)$ nC] beams are critical for some experiments on wakefield acceleration using small-aperture structures (operating at sub-THz frequencies) and phase-space manipulations investigated at AWA [5–7] . Likewise, high-charge bunches require a moderate emittance with low energy spread to minimize chromatic aberrations associated with the final focusing in the PETS structure. Most of the intial conditions and accelerator settings can be continuously varied except for the initial photocathode-laser distribution which can either be approximated as a single Gaussian distribution (refer to as "1G") with ~ 400-fs (FWHM) duration or a plateau flat-top distribution ("FT") produced by stacking 32 Gaussian pulses using five α-BBO crystals with ~ 6-ps (FWHM) duration [8]; see Fig. 1(b) and (c) respectively.

The POISSON/SUPERFISH suite was used to generate the on-axis magnetic fields for the solenoidal lenses and RF fields for the RF gun and linac cavities. The beam dynamics simulations were performed using the ASTRA program using the cylindrical-symmetric space-charge algorithm. Our simulation conservatively used the low-energy settings of the linac where only four or the six accelerating cavities are powered. The optimizations were performed with the DEAP evolutionary computation framework [9]. During the optimization the 12 control parameters included the laser transverse size on the photocathode, the phase and amplitude of the RF gun and two first accelerating cavities, the peak values of 4 solenoids (the 3 solenoids surrounding the RF gun and one solenoid downstream of the first accelerating cavity) and the matching solenoid position.

RESULTS

Optimization for Ideal Case

Figure 2 summarizes the Pareto fronts in the $(\varepsilon_\perp, \sigma_E)$ domain resulting from the optimization for all of the 8 considered configurations. Two clusters of Pareto fronts

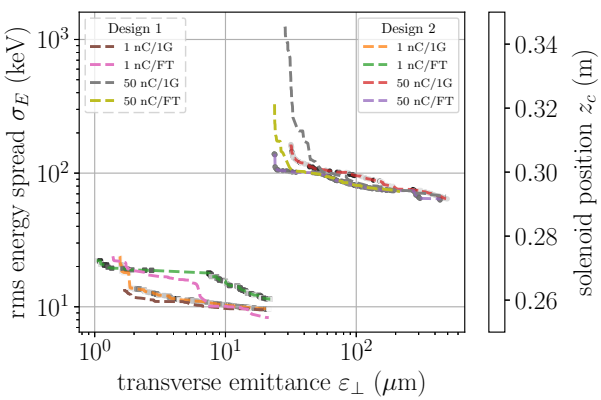

Figure 2: Pareto fronts obtained for both solenoid Designs 1 and 2 for the two cases of laser temporal profiles ("1G" and "FT") and bunch charges (1 and 50 nC).

emerge from the latter Figure. One of them in the domain ($\varepsilon_\perp \in [1, 20]$ μm and $\sigma_E \in [10, 30]$ keV) corresponds to bunch charges $Q = 1$ nC. The other group of Pareto fronts in the domain ($\varepsilon_\perp \in [30, 400]$ μm and $\sigma_E \in [70, 1000]$ keV) is associated with $Q = 50$ nC. Despite the disparity in $\varepsilon_\perp$ and σ_E values associated with the two cases of charges, the optimizations indicate that Design 2 offers some compromise where acceptable tradeoffs can be reached for a common fixed solenoid position.

Specifically, we fixed the solenoid position to $z_s = 0.287$ m from the photocathode following an analysis of Fig. 2 and performed a multi-objective optimization where all the parameters previously listed but the solenoid position are used as variables. Figure 3 presents the corresponding

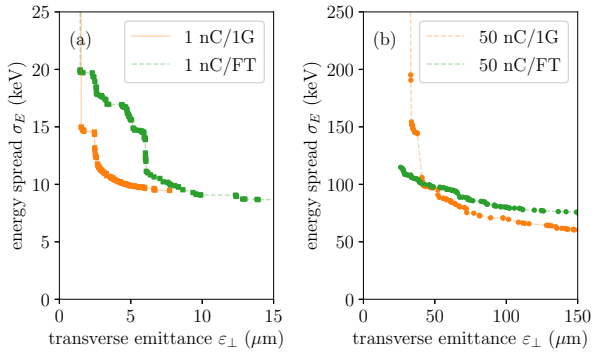

Figure 3: Pareto fronts for "Design 2" solenoid located at $z_s = 0.287$ m for the 1-nC (a) and 50-nC (b) bunch charges.

Pareto fronts and confirms that emittance values close to ~ 1 μm can be attained for $Q = 1$ nC. Likewise, the high-charge optimizations indicate that $(\varepsilon_\perp, \sigma_E) \leq (100$ μm, 100 keV) are achievable at ~ 40 MeV. The corresponding relative energy spread is $\sigma_E/E < 2.5\times10^{-3}$ which should significantly reduce chromatic aberrations. Additionally, the optimization gives lower energy spread value for given emittance value for the "1G" laser-configuration at $Q = 1$ nC while reaching lower emittance favors the "FT" laser for $Q = 50$ nC. The latter is expected as photo-emitting an electron bunch with a short laser pulse usually results in a space-charge dominated beam expansion which produces significant correlated energy spread [10, 11].

To further examine the beam quality we selected a few settings and analyzed the corresponding beam evolution along the injector beamline. Figures 4 and 5 present the evolution of key beam parameters along the beamline for respectively a 1-nC and 50-nC bunch. For both cases we selected the 1G laser distribution with both configurations reaching a final kinetic energy $K \simeq 40$ MeV. The 1-nC case reaches transverse emittance $\varepsilon_\perp \simeq 1.5$ μm. Likewise, it is worth noting that the 50-nC case produces a peak current $\hat{I} \simeq cQ/(\sqrt{2\pi}\sigma_z) \sim 2.5$ kA without any compression while maintaining a transverse emittance $\varepsilon_\perp \simeq 60$ μm. These parameters will further improve by optimizing the linac with all six cavities powered.

ISBN: 978-3-95450-227-1 ISSN: 2673-5490 doi:10.18429/JACoW-IPAC2022-WEPOPT065

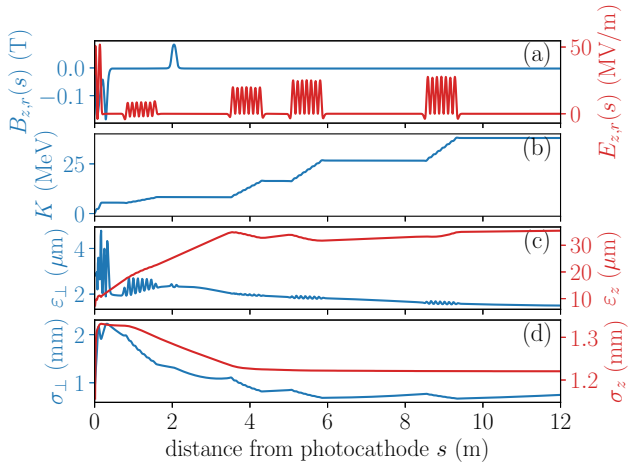

Figure 4: Evolution of beam parameters along the beamline for the case of a 1-nC bunch with the 1G laser distribution. The beamline external accelerating (E_z) and focusing (B_z) fields experienced by the reference particle appear in (a). The parameters are the kinetic energy K (b), the transverse and longitudinal ε_z emittances (c) and the transverse $\sigma_\perp$ beam size and bunch length σ_z (d).

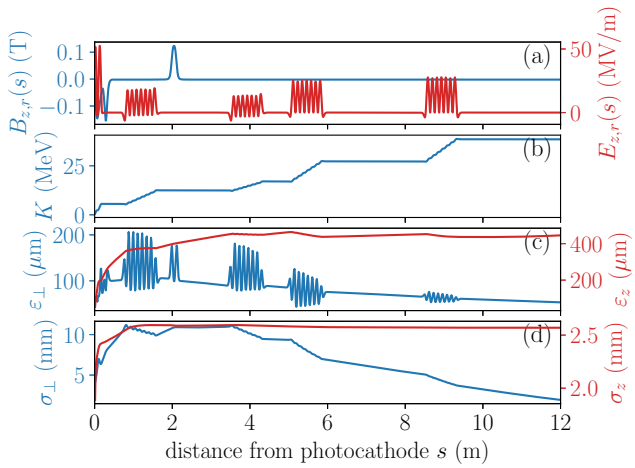

Figure 5: Evolution of beam parameters along the beamline for the case of a 50-nC bunch with the 1G laser distribution. The plots description is similar to Fig. 4.

Impact of Multipoles field in Solenoid

Owing to the fabrication process solenoid magnets do not possess an axial-symmetry. Such an asymmetry can significantly affect the beam's transverse emittances. Consequently, it is instructive to assess the impact of non-ideal multipole contributions to the field [12]. We perform such an investigation by considering the dipole and quadrupole fields. We consider the optimized configuration presented in Fig. 4 and overlap a quadrupole or a dipole magnet to the matching solenoid in the ASTRA model. The beam distribution is tracked up to the photoinjector's end (at $z = 12$ m) and the emittances recorded. Figure 6 summarizes the impact of these dipole and quadrupole fields on the the averaged emittance $\tilde{\varepsilon} \equiv \sqrt{\varepsilon_x \varepsilon_y}$ defined as the geometric average of the horizontal and vertical emittances. Imposing the relative emittance dilution to be below 5% requires the quadrupole gradient integral $\int G d\ell \leq 2.5$ G and dipole field integral $\int B d\ell \leq 0.3$ G.m for a nominal magnetic field of $|\hat{B}_z| = 0.186$ T. These multipoles can also be partially corrected by a set of normal-skew quadrupole magnets [13].

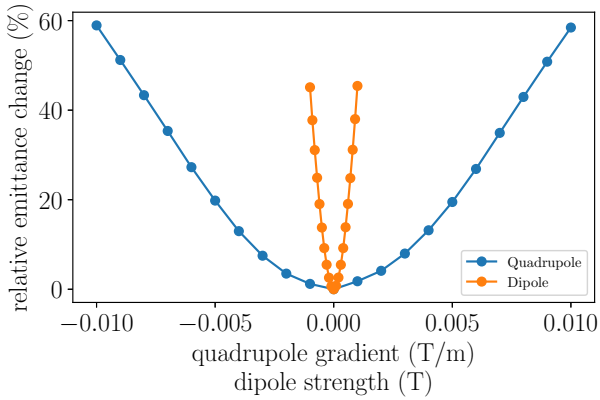

Figure 6: Relative average-emittance ($\tilde{\varepsilon}$) dilution as a function of dipole and quadrupole field strength (the peak field for the matching solenoid is $|\hat{B}_z| = 0.186$ T).

CONCLUSION

This paper summarizes the optimization study that was performed to investigate the impact of two different solenoid designs on emittance and energy spread. Our optimization revealed that the bore size of the solenoid did not greatly affect the beam parameters as both solenoid designs yielded similar tradeoff curves between emittance and energy spread. Given that the smaller-bore solenoid would require a special EVAC® chain-clamp flange to accommodate its installation while the larger-bore solenoid ("Design 2") can be slid over a standard flange, "Design 2" was selected. We correspondingly investigated the performances of beamline configurations implementing this solenoid and show emittance ~ 1.5 µm could be attained at 1 nC. Further work will explore possible optimization of the linac position, consider 3D maps of the electromagnetic fields (as the current simulations assume axially-symmetric fields in RF cavities), and explore the impact of short-range wakefield effects.

ACKNOWLEDGMENTS

We thank Tianzhe Xu (NIU) for sharing his implementation of the DEAP optimizer with ASTRA. This work was performed under the Chicagoland Accelerator Science Traineeship (CAST) program sponsored by the U.S. DOE award DE-SC0020379 to the Illinois Institute of Technology and Northern Illinois University (NIU). XL and PP are partially supported by DOE award DE-SC0022010 to NIU. The work by the AWA team is sponsored under DOE contract No. DE-AC02-06CH11357 with Argonne National Laboratory.

ISBN: 978-3-95450-227-1 ISSN: 2673-5490 doi:10.18429/JACoW-IPAC2022-WEPOPT065

REFERENCES

[1] J. Power, M. Conde, W. Gai, Z. Li, and D. Mihalcea, "Upgrade of the Drive LINAC for the AWA Facility Dielectric Two-Beam Accelerator," in *Proceedings1st International Particle Accelerator Conf. (IPAC'10)*, Japan, paper THPD016, 2010.

[2] W. H. Tan, S. Antipov, D. S. Doran, G. Ha, C. Jing, E. Knight, S. Kuzikov, W. Liu, X. Lu, P. Piot, J. G. Power, J. Shao, C. Whiteford, and E. E. Wisniewski, "Demonstration of sub-GV/m Accelerating Field in a Photoemission Electron Gun Powered by Nanosecond *X*-Band Radiofrequency Pulses," 2022. arXiv:2203.11598

[3] J. H. Shao *et al.*, "Demonstration of Gradient Above 300 MV/m in Short Pulse Regime Using an X-Band Single-Cell Structure," presented at IPAC22, Bangkok, Thailand, Jun. 2022, paper FROXSP2, this conference.

[4] G. Ha, K.-J. Kim, J. G. Power, Y. Sun, and P. Piot, "Bunch shaping in electron linear accelerators," *Rev. Mod. Phys.*, vol. 94, p. 025006, May 2022.

[5] G. Ha, M. H. Cho, W. Namkung, J. G. Power, D. S. Doran, E. E. Wisniewski, M. Conde, W. Gai, W. Liu, C. Whiteford, Q. Gao, K.-J. Kim, A. Zholents, Y.-E. Sun, C. Jing, and P. Piot, "Precision control of the electron longitudinal bunch shape using an emittance-exchange beam line," *Phys. Rev. Lett.*, vol. 118, p. 104801, Mar 2017.

[6] A. Halavanau, Q. Gao, M. Conde, G. Ha, P. Piot, J. G. Power, and E. Wisniewski, "Tailoring of an electron-bunch current distribution via space-to-time mapping of a transversely shaped, photoemission-laser pulse," *Phys. Rev. Accel. Beams*, vol. 22, p. 114401, Nov 2019.

[7] T. Xu, D. S. Doran, W. Liu, P. Piot, J. G. Power, C. Whiteford, and E. Wisniewski, "Demonstration of eigen-to-projected emittance mapping for an ellipsoidal electron bunch," *Phys. Rev. Accel. Beams*, vol. 25, p. 044001, Apr 2022.

[8] J. G. Power and C. Jing, "Temporal laser pulse shaping for rf photocathode guns: The cheap and easy way using uv birefringent crystals," *AIP Conference Proceedings*, vol. 1086, no. 1, pp. 689–694, 2009.

[9] F.-A. Fortin, F.-M. De Rainville, M.-A. Gardner, M. Parizeau, and C. Gagné, "DEAP: Evolutionary algorithms made easy," *Journal of Machine Learning Research*, vol. 13, pp. 2171–2175, jul 2012.

[10] O. J. Luiten, S. B. van der Geer, M. J. de Loos, F. B. Kiewiet, and M. J. van der Wiel, "How to realize uniform three-dimensional ellipsoidal electron bunches," *Phys. Rev. Lett.*, vol. 93, p. 094802, Aug 2004.

[11] P. Piot, Y.-E. Sun, T. J. Maxwell, J. Ruan, E. Secchi, and J. C. T. Thangaraj, "Formation and acceleration of uniformly filled ellipsoidal electron bunches obtained via space-charge-driven expansion from a cesium-telluride photocathode," *Phys. Rev. ST Accel. Beams*, vol. 16, p. 010102, Jan 2013.

[12] D. H. Dowell, F. Zhou, and J. Schmerge, "Exact cancellation of emittance growth due to coupled transverse dynamics in solenoids and rf couplers," *Phys. Rev. Accel. Beams*, vol. 21, p. 010101, Jan 2018.

[13] L. Zheng, J. Shao, Y. Du, J. G. Power, E. E. Wisniewski, W. Liu, C. E. Whiteford, M. Conde, S. Doran, C. Jing, C. Tang, and W. Gai, "Experimental demonstration of the correction of coupled-transverse-dynamics aberration in an rf photoinjector," *Phys. Rev. Accel. Beams*, vol. 22, p. 072805, Jul 2019.